


Article

Bionic Design of Liquid Fertilizer Deep Application Spray Needle, Based on Badger Claw-Toe, for Improving the Operating Performance of Liquid Fertilizer Deep Application in Northeast China

Wenqi Zhou ¹, Xue Ni ¹, Nuan Wen ¹, Tianhao An ¹ and Yijia Wang ^{2,*} ¹ College of Engineering, Northeast Agricultural University, Harbin 150030, China² Department of Industrial and Manufacturing Systems Engineering, The University of Hong Kong, Hong Kong 999077, China

* Correspondence: yijia.wang@connect.hku.hk; Tel.: +86-166-2097-4902

Abstract: Deep application of liquid fertilizer is a technique that applies liquid fertilizer deep near the root system of crops, which has many advantages such as high fertilizer utilization rate and low environmental pollution. However, high power and high specific energy consumption caused by soil-engaging components in liquid fertilizer deep application make it difficult to popularize in northeast China. The claw-toe structure of burrowing animals has the characteristics of low resistance and low friction, which has been the focus of many scholars' research on soil-engaging components. The claw-toe structure of the badger, a widely distributed burrowing animal in northeast China, has good characteristics of low power and low specific energy consumption. Therefore, in this research, a bionic liquid fertilizer deep application spray needle was designed, based on the claw-toe structure of the badger, to improve the operating performance of liquid fertilizer deep application. In this research, the discrete element method (DEM) was used for a computer simulation test, and the indoor soil bin verification test was carried out. The results showed that the operating angle, operating speed and fertilization depth of bionic liquid fertilizer deep application spray needle had significant effects on the power and specific energy consumption, and the optimal operating performance combination of bionic liquid fertilizer deep application spray needle was obtained as follows: The fertilization depth is 60 mm; the operating speed is 6 km h⁻¹; the operating angle is 24.8°; the power consumption is 0.066 kW; and the specific energy consumption is 4.257 kJ m⁻³ under this operating condition. Through the comparison of operating performance, the operating performance of the bionic liquid fertilizer deep application spray needle is significantly better than that of other types of liquid fertilizer deep application furrow opener, with the power reduced by 9.52–40.5% and the specific energy consumption reduced by 93.9–208.6%. This research clarified the internal mechanism affecting the operating performance. Finally, based on the above findings, this research suggests that more attention should be paid to finding suitable bionic prototype and design scheme in the future design and research of soil-engaging components of liquid fertilizer deep application.



Citation: Zhou, W.; Ni, X.; Wen, N.; An, T.; Wang, Y. Bionic Design of Liquid Fertilizer Deep Application Spray Needle, Based on Badger Claw-Toe, for Improving the Operating Performance of Liquid Fertilizer Deep Application in Northeast China. *Processes* **2023**, *11*, 756. <https://doi.org/10.3390/pr11030756>

Academic Editor: Elisa Gamalero

Received: 10 February 2023

Revised: 26 February 2023

Accepted: 27 February 2023

Published: 3 March 2023



Copyright: © 2023 by the authors. Licensee MDPI, Basel, Switzerland. This article is an open access article distributed under the terms and conditions of the Creative Commons Attribution (CC BY) license (<https://creativecommons.org/licenses/by/4.0/>).

Keywords: liquid fertilizer deep application technology; bionic design; fertilizer spray needle; DEM

1. Introduction

Black land is a valuable resource for all human beings and is known as “the most fertile soil in the world”; it is mainly distributed in Ukraine Plain, the Mississippi Plain of the United States, Northeast China Plain and the Pampas Plain of South America, etc., with many advantages, such as high fertility and rich humus content [1–3]. With the improvement of human production and living standards, the applying quantity of chemical fertilizers has increased dramatically in most countries around the world, and the long-term excessive application of chemical fertilizers has caused many environmental problems,

such as the decrease of soil fertility, the destruction of soil aggregate structure and the pollution of water environment [4–7]. Therefore, curbing the excessive application of chemical fertilizers can effectively protect the valuable black land resources [8,9].

Liquid fertilizer deep application technology is a kind of fertilization technology in which liquid fertilizer is applied deeply in the furrow by furrowing with soil-engaging components such as ploughs, furrow openers or fertilizer spray needles, followed by covering [10,11]. Compared with solid fertilizer spreading and liquid fertilizer spraying, liquid fertilizer deep application technology has higher fertilizer utilization rate and significantly reduces environmental pollution [12]. In the process of liquid fertilizer deep application, reducing the power consumption and specific energy consumption of soil-engaging components on traction equipment is an important issue to be solved in the liquid fertilizer deep application operating environment [13,14]. The structure, size and surface shape of the soil-engaging components have a significant impact on the power and specific energy consumption during the operation of the soil-engaging components [15]. Obviously, if a high-efficiency liquid fertilizer deep application soil-engaging component with low power and low specific energy consumption can be developed and designed, it can significantly promote the promotion of liquid fertilizer deep application technology in northeast China.

There are many organisms in nature that have biological structures with low resistance and low friction characteristics [16,17]. With the continuous development of human technology, their special biological structures can be extracted, improved and optimized by modern means to provide services for human production and life [18]. Many research scholars have found that the claw-toe structure of burrowing animals, which are widely distributed in northeastern China, has a significant drag reduction effect [19,20], which is due to its special multi-extreme value curve structural characteristics that can achieve low disturbance characteristics to the soil. If this structure is replicated on the liquid fertilizer deep application spray needle, it can effectively improve the operating performance of the liquid fertilizer deep application spray needle.

Currently, many scholars have conducted bionic design and research on the soil-engaging low resistance characteristics of organisms. Shuhong et al. [21] extracted and studied the head curve of sailfish by bionic technology and designed a new bionic sharp-angle furrow opener, which has significant drag reduction and low disturbance performance. Wang et al. [22] designed a new bionic furrow opener, by extracting biological features of soil species (dung beetles and pangolins) and coupling them with the furrow opener structure, and conducted virtual simulation tests. Lee et al. [23] designed a new soil drilling mechanism by extracting the head structure and the outer contour of the front claw-toe of the eastern mole, and the optimal combination was obtained through experiments to improve the mechanical performance of the drilling mechanism. Wang et al. [24] designed four kinds of bionic sturgeon liquid fertilizer deep application furrow openers based on the streamlined body shape curve of sturgeon and combined with the principle of bionics, and they verified the mechanism of low furrowing resistance and high backfill rate of the bionic structure of fish body curve through the indoor soil bin test. Sun et al. [25] designed a bionic bear claw soil tillage device with low resistance and low friction based on the characteristics of red soil by extracting the bear claw structure. The optimal parameter combination was obtained through the DEM virtual simulation test and compared with the conventional tillage device through the indoor soil barn test. The bionic bear claw soil tillage device has excellent tillage performance. Many scholars have used bionic technology to do a lot of research on the application of soil-engaging components, but most of the research centers on the extraction of the curve structure of the surface of biological features, while less research is done on the extraction and application research of the overall structure of biology.

In this research, the bionic technology was used for the sampling and biological feature extraction of the claw-toe structure of burrowing badgers, widely distributed in northeast China, and the bionic liquid fertilizer deep application spray needle was designed. Meanwhile, the DEM virtual simulation model of black soil was established, and the

performance optimization test of the bionic liquid fertilizer deep application spray needle was carried out. The accuracy of DEM virtual simulation test results was verified through indoor soil bin tests, and the internal mechanism of low power consumption and low specific energy consumption of the badger claw-toe structure was clarified. This research can provide a new design idea and method for the design of a bionic liquid fertilizer deep application spray needle, can promote the use of liquid fertilizer deep application technology in northeast China and can protect the valuable black land resources in this area, which is of great significance.

2. Materials and Methods

2.1. DEM Virtual Simulation

2.1.1. Soil DEM Virtual Simulation Model Construction

In this research, the black soil of corn growing areas in northeast China was sampled and measured. On 25 June 2022, the experimental plot (126°58'31" N, 45°32'29" E) of Northeast Agricultural University, Achen District, Harbin City, Heilongjiang Province, China was sampled to determine the soil parameters, as shown in Table 1, which was used to construct the DEM virtual simulation model.

Table 1. Parameter list of DEM virtual simulation test model.

Parameter	Value
Soil unit particle size mm	2~3
Soil density $\text{g}\cdot\text{cm}^{-3}$	1.516
Poisson's ratio of soil	0.39
Shear modulus of soil MPa	1.00
Coefficient of static friction between soil particles	0.53
Coefficient of dynamic friction between soil particles	0.78
Coefficient of recovery between soil grains	0.23
Surface energy density $\text{J}\cdot\text{m}^{-2}$	5.50
Static friction coefficient between soil and 65 Mn	0.47
Coefficient of rolling friction between soil and 65 Mn	0.11
Collision recovery coefficient between soil and 65 Mn	0.09

2.1.2. Soil Bin DEM Virtual Simulation Model Construction

EDEM 2020 software was used to construct spherical particles as a virtual soil unit model [26]. The overall size of the virtual soil unit is determined to be 2000 mm \times 400 mm \times 140 mm, where a 1000 mm area ensures soil balance. The 700 mm area is used for data collection. The 300 mm area is used to eliminate the data error caused when the bionic liquid fertilizer deep application spray needle breaks away from the virtual soil bin, and the 100 mm collection area is added on both sides of the soil bin to collect the transversely thrown soil units [27], as shown in Figure 1. Before the experiment, the bionic liquid fertilizer deep application spray needle was imported into the virtual environment to simulate the required operating depth and operating speed.

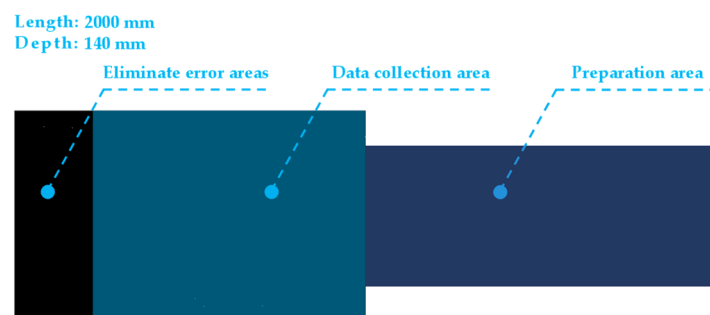


Figure 1. Schematic diagram of the soil bin DEM virtual simulation model.

2.2. Test Equipment

An industrial-grade 3D scanner (OKIO 5M, Beijing Tianyuan 3D Technology Co., Ltd., Beijing, China) was selected as the test equipment to extract the biological features, as shown in Figure 2a. A laser sintering 3D printer (M420, precision 0.005 mm, Shanghai Liantai Technology Co., Ltd., Shanghai, China) was selected to carry out the 3D printing of soil-engaging components of the bionic liquid fertilizer deep application spray needle, as shown in Figure 2b. The DEM virtual simulation test was conducted by a work station (Saver Blade 7000 III, Beijing Legend Holdings Co., Ltd., Beijing, China), and the DEM virtual simulation test process is shown in Figure 2c. The indoor soil bin test was carried out in the Sowing Combined Harvest Laboratory, College of Engineering, Northeast Agricultural University (126°43'25" N, 45°44'27" E, Harbin, Heilongjiang Province, China), and the test equipment consisted of a trolley, a frequency conversion cabinet (model F1000-G055T3C, Eura Drives Electric Co., Ltd., Yantai, China), three-phase asynchronous motor (Y2-10L-4 type, Yongce Mechanical Equipment Co., LTD., Shanghai, China) and tensile pressure gauge (DS2-S type, Zhiqu Precision Instrument Co., LTD., Dongguan, China), the frequency conversion cabinet drives the travel motor and changes the speed of the travel motor by modifying the frequency of the frequency conversion cabinet to control the reciprocating motion of the test dolly on the soil trough guide to obtain the operating speed of the bionic liquid fertilizer deep application fertilizer spray needle, as shown in Figure 2d.

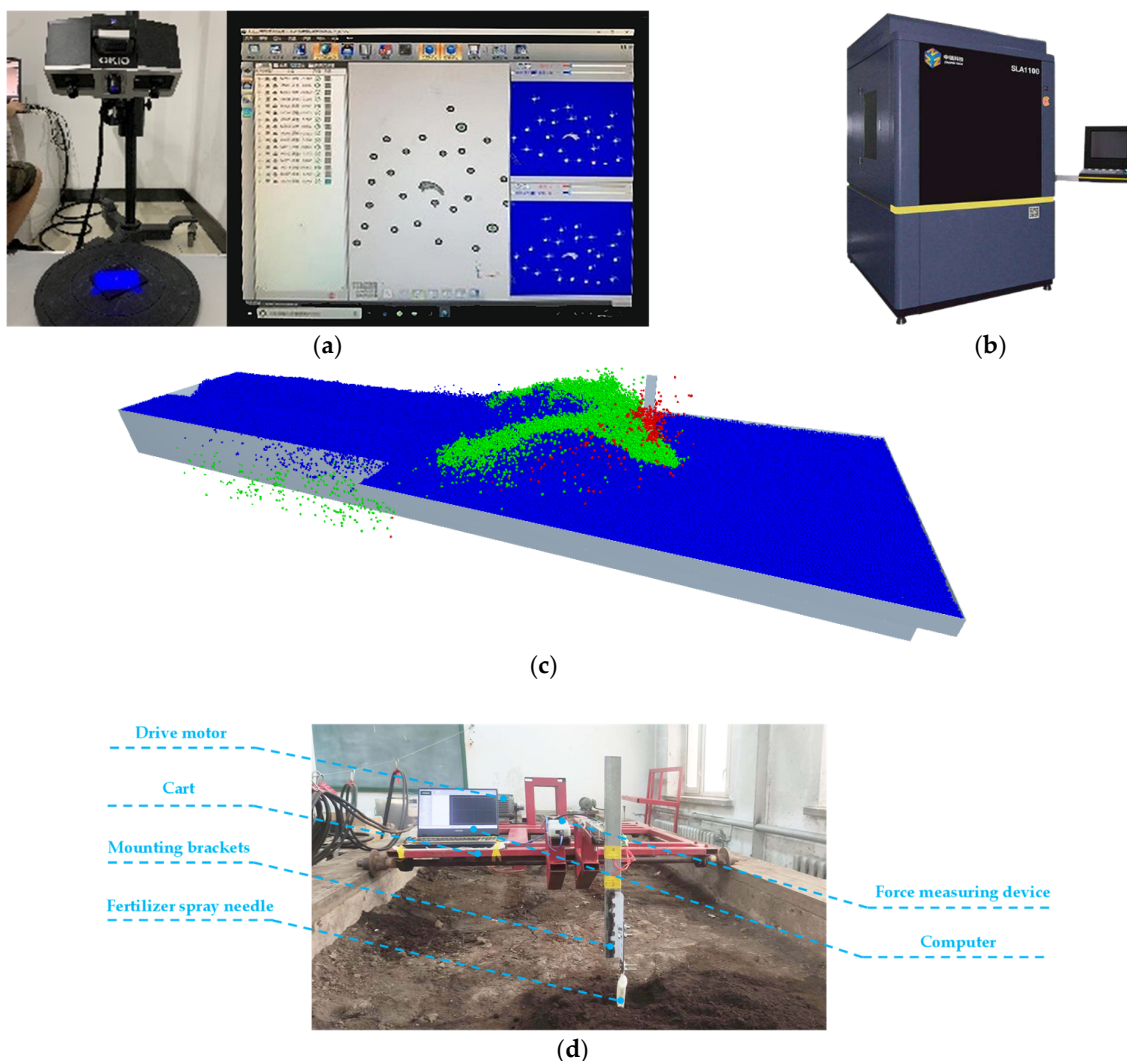


Figure 2. Schematic diagram of test equipment. (a) Industrial-grade 3D scanner; (b) laser sintering 3D printer; (c) DEM virtual simulation test process; (d) indoor soil bin test bench.

2.3. Design of Bionic Liquid Fertilizer Deep Application Spray Needle

The badger is an animal of the family Mustelidae, genus *Badger*, with a relatively wide range of habitats, such as forests, thickets, fields and lakes, and is distributed in most parts of the Asian and Eurasian continent [28]. The badger digs a burrow to live in while hibernating, and the burrow tunnel is several tens of meters long with smooth and neat walls, which can show that its claw-toe structure has the biological characteristic of drag reduction and disturbance reduction. Figure 3a shows a badger digging a burrow [29]. In this research, a naturally dead 5-year-old male badger specimen from captive breeding in northeast China was selected and its forepaw middle finger claw toe was disinfected by placing it in ethanol solution with a volume fraction of 28%. After soaking for 2–3 h, it was washed 20 times repeatedly using distilled water and, finally, placed in a beaker to dry naturally at room temperature, as shown in Figure 3b. According to the depth requirement of 50–80 mm for deep liquid fertilizer application operation in mid-tillage of a corn crop in northeast China, the basic size was enlarged by 10 times to control the height of the fertilizer spraying needle of 105 mm in order to ensure that the liquid fertilizer deep application spraying needle meets the depth requirement while retaining the installation length of the fertilizer application tube. Finally, the Geomagic Design X software was used to sample, smooth and eliminate miscellaneous points in order to improve the quality of the point cloud model, as shown in Figure 3c.



Figure 3. Bionic biological prototype and extraction process. (a) Badger burrowing process; (b) extraction process of badger claw-toe structure; (c) badger claw-toe model.

Design of Bionic Liquid Fertilizer Deep Application Spray Needle and Mounting Bracket

In order to make the bionic liquid fertilizer deep application spray needle spray liquid fertilizer in time during the operation, the badger claw toe was designed as a hollow structure as a liquid fertilizer spraying pipeline. In order to facilitate the installation in the field operation, a demountable bracket with adjustable angle was designed. The mounting hole is used to install the mounting bracket on the rack of the traction equipment. Adjusting the connecting hole to adjust the operating angle of the spray needle, the connecting hole is connected with the spray needle rack. The connection port of the fertilizer spraying pipeline, the fertilizer spraying pipeline and the fertilizer spray needle port are used to spray liquid fertilizer. The bionic liquid fertilizer deep application spray needle is made of photosensitive resin material as a whole, as shown in Figure 4a. The operating angles of the bionic liquid fertilizer deep application spray needle were adjusted to 0° , 22.5° and 45° [30], as shown in Figure 4b.

2.4. DEM Virtual Simulation Test Design

2.4.1. Single-Factor Experimental Design

Referring to the requirements of mid-tillage fertilizer application for maize crops in northeastern China and related scholarly studies [24,31,32], the operating speed (5, 6, 7, 8, 9, 10 and 11 km h^{-1}) and the depth of application (55, 60, 65, 70, 75, 80 and 85 mm) were selected as the test factors for the single-factor test.

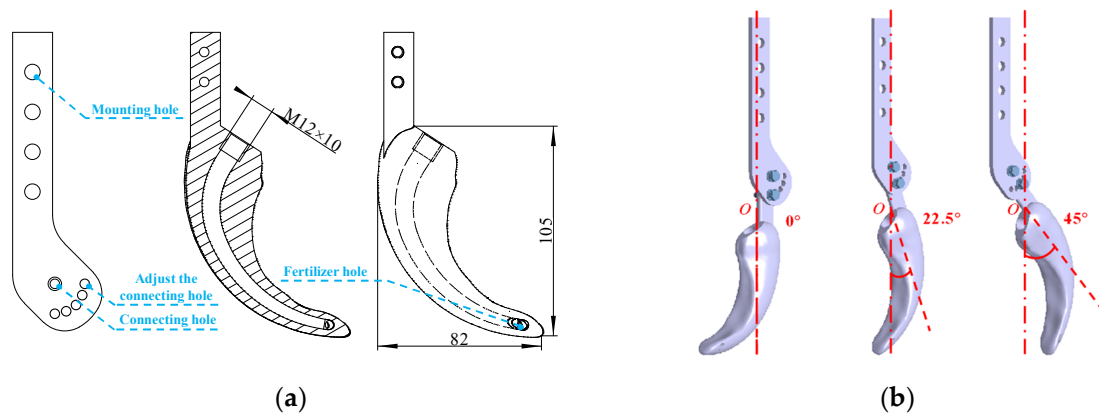


Figure 4. Schematic diagram of bionic liquid fertilizer deep application spray needle and operating angle. (a) Schematic diagram of bionic liquid fertilizer deep application spray needle and mounting bracket; (b) schematic diagram of operating angle adjustment.

2.4.2. Multi-Factor Experimental Design

Based on the single-factor test, the parameters of the bionic liquid fertilizer deep application spray needle were optimized by a BOX-Behnken three-factor, three-level experimental design. The operating angles A (0 , 22.5° and 45.0°), operating speeds B (6 , 8 and 10 km h^{-1}) and application depths C (60 , 70 and 80 mm) were selected as test factors, and the power P and specific energy consumption Q were used as test indicators.

2.4.3. Determination of Test Indexes

In this research, the power parameter P and the specific energy consumption parameter Q were selected as the test indexes of the DEM virtual simulation test for bionic liquid fertilizer deep application fertilizer spray needle, and the power parameter P , kW was determined by Equation (1)

$$P = \frac{Fv}{1000} \quad (1)$$

where v is the operating speed of the bionic liquid fertilizer deep application spray needle, m s^{-1} . F is the average operating horizontal resistance of the bionic liquid fertilizer deep application spray needle in the data collection area, N.

The specific energy consumption parameter Q , kJ m^{-3} is determined by Equation (2)

$$Q = \frac{W}{V} = \frac{FL}{SL} = \frac{F}{S} \quad (2)$$

where W is the energy consumption, kJ. V is the volume of soil disturbance, m^3 . L is the operating distance of bionic liquid fertilizer deep application spray needle, mm. S is the gully cross-sectional area (soil disturbance cross-sectional area), mm^{-2} .

In this research, the porosity grid box was used to extract the soil disturbance cross-sectional area of the operation of bionic liquid fertilizer deep application spray needle in DEM virtual simulation test [33].

2.5. Design of Indoor Soil Bin Verification Test

In July 2022, the test was conducted in the Agricultural and Animal Husbandry Machinery Laboratory of Northeast Agricultural University ($126^\circ 43' 25'' \text{ N}$, $45^\circ 44' 27'' \text{ E}$) to verify the accuracy of the DEM virtual simulation test model and the rationality of the optimization of the bionic liquid fertilizer deep application fertilizer spray needle. The accuracy of the DEM virtual simulation model was verified by three replications with the results of optimized parameters: the operating depth of 60 mm , operating speed of 6 km h^{-1} and operating angle of 24.8° of the liquid fertilizer deep application furrow opener.

During the test, black soil from the corn-growing area of northeast China was selected as the soil in the soil bin. Organisms, weeds and stones in the soil were sieved through a round hole sieve. Water was sprayed on the soil, according to the actual field conditions, to adjust the soil moisture content, and the ridge was built. Soil conditions and parameter indexes are shown in Figure 5a. The operating resistance parameters in the test were obtained by the tensile pressure gauge; the catastrophe points were removed; and the average operating resistance values were collected from the data as the operating resistance parameters under the operating conditions. After the operation of the bionic liquid fertilizer deep application spray needle, the outer layer gully contour was photographed and depicted. After the gully contour was obtained, the loose soil was removed by brush and then the gully was depicted twice. The area measurement was performed after combining the results of the two depictions as the soil disturbance area parameter under this operation condition, and the process is shown in Figure 5b.

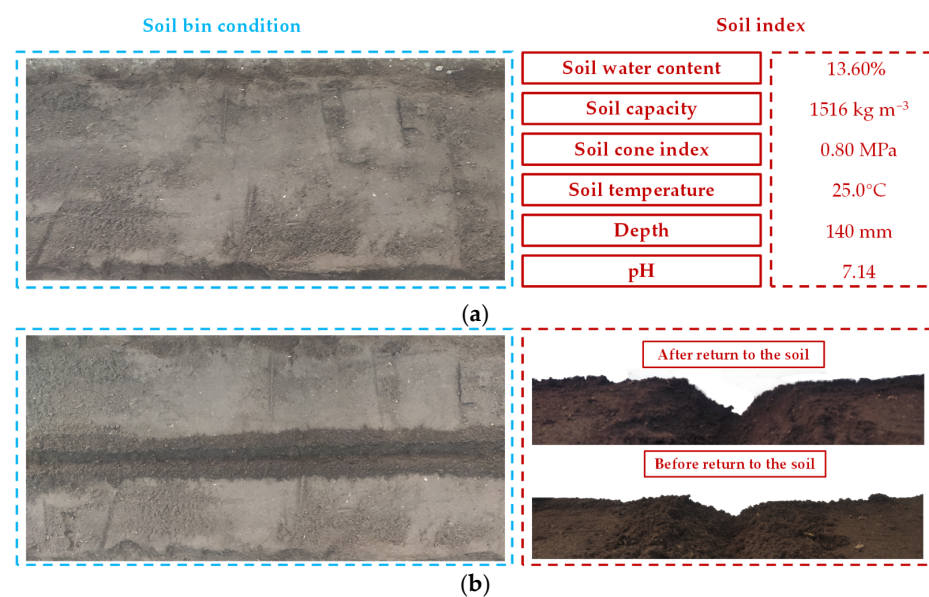


Figure 5. Indoor soil bin conditions and test process. (a) Soil conditions and parameters of the indoor soil bin test; (b) extraction process and results of soil gully contour parameters.

3. Results

3.1. The Effect of Operating Speed on Power and Specific Energy Consumption

In the DEM virtual simulation test, the relationship between power, specific energy consumption and operating speed under the condition of an 80 mm fertilizer application depth is shown in Figure 6. The resistance during the operation of the bionic liquid fertilizer deep application of the fertilizer spray needle mainly comes from the impact of soil particles, with the increase in operating speed, the relative speed of soil particles and fertilizer spray needle increases, the power consumption in the disengagement of the bionic liquid fertilizer deep application of fertilizer spray needle will also increase, then the power and specific energy consumption both increase. Figure 6a shows that the trend of power consumption at 0°, 22.5° and 45° is basically the same, with the operating speed increasing from 4 km h⁻¹ to 12 km h⁻¹ and the power consumption being the highest at 45°. Forty-five-degree power increases from 0.066 kW to 0.257 kW with a growth rate of 290.53%. Zero-degree and 22.5° power increases from 0.077 kW and 0.103 kW to 0.242 kW and 0.316 kW for 0° and 22.5° operating conditions, respectively, with growth rates of 215.00% and 208.64%. In Figure 6b, it is shown that the specific energy consumption decreased from 5.063 kJ m⁻³ to 3.718 kJ m⁻³ with a 36.19% decrease as the operating speed increased from 6 km h⁻¹ to 8 km h⁻¹ under 0° operating conditions and increased to 5.499 kJ m⁻³ with a 47.92% increase after the operating speed increased to 10 km h⁻¹. At 22.5°, the specific energy consumption increased from 4.110 kJ m⁻³ to 6.034 kJ m⁻³, with

a growth rate of 75.70%. The specific energy consumption increased from 3.483 kJ m^{-3} to 8.969 kJ m^{-3} at 45° , with a growth rate of 157.53%. 45° operating conditions showed the largest increment in the specific energy consumption parameter. As can be seen from Figure 6b, when the operating speed is in the range of $6\text{--}10 \text{ km h}^{-1}$ and the angle of soil entry is 45° , the specific energy consumption parameter first decreases and then increases, then the operating speed is in the range of $6\text{--}10 \text{ km h}^{-1}$ as the optimal speed interval for liquid fertilizer deep application operation.

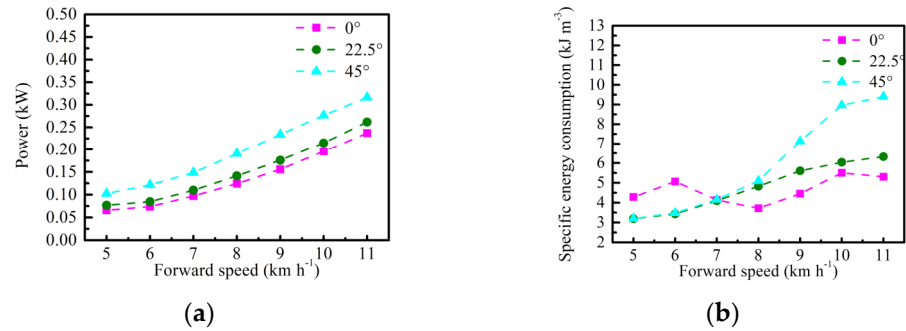


Figure 6. Effect of operating speed on power and specific energy consumption; (a) effect of operating speed on power; (b) effect of operating speed on specific energy consumption.

3.2. The Effect of Operating Depth on Power and Specific Energy Consumption

In the experiment, the relationship between power and specific energy consumption under the operating speed of 10 km h^{-1} is shown in Figure 7. As shown in Figure 7a, the power increased gradually at 0° , 22.5° and 45° with the increase of fertilizer application depth. The specific energy consumption increased and then decreased at 22.5° and 45° , and the specific energy consumption parameter increased, then decreased and finally increased at 0° . When the fertilizer application depth increased from 55 mm to 85 mm , the power parameter increased the most in 45° operation condition from 0.191 kW to 0.292 kW , with a growth rate of 52.99%. Zero-degree and 22.5° conditions increased from 0.129 kW and 0.129 kW to 0.202 kW and 0.235 kW , respectively, with a growth rate of 91.67% and 82.95%. As shown in Figure 7b, the specific energy consumption parameter increased and then decreased for both 22.5° and 45° conditions from 6.304 kJ m^{-3} and 8.475 kJ m^{-3} to 6.830 kJ m^{-3} and 9.632 kJ m^{-3} , respectively, with growth rates of 8.33% and 13.66%, when the operating depth increased from 55 mm to 85 mm . At 0° , the specific energy consumption increased from 4.205 kJ m^{-3} to 6.015 kJ m^{-3} when the working depth increased from 55 mm to 85 mm , with an overall growth rate of 43.07%. The maximum specific energy consumption parameter was found at 45° operating conditions. As can be seen from Figure 7b, when the operating depth is in the range of $60\text{--}80 \text{ mm}$, the angle of the figure is 45° , the specific energy consumption parameter increases first and then decreases, and then the operating depth in the range of $60\text{--}80 \text{ mm}$ is the optimal depth interval for liquid fertilizer deep application operation.

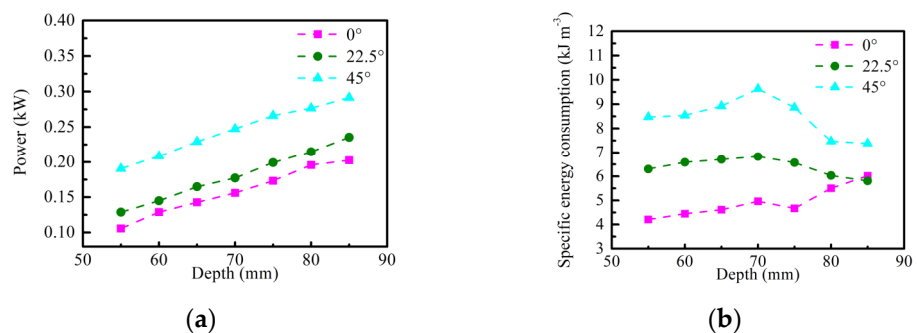


Figure 7. Effect of operating depth on power and specific energy consumption. (a) Effect of operating speed on power; (b) effect of operating depth on specific energy consumption.

3.3. The Relationship between Power, Operating Angle, Operating Depth and Operating Speed

As shown in Figure 8a–c, when operating depth remains constant, the power increases with the increase of operating speed and angle. At the operating depth of 70 mm and the operating speed of 6 km h⁻¹, the operating angle increases from 0° to 45°, and the power increases from 0.063 kW to 0.102 kW, with a growth rate of 61.90%. At the operating depth of 70 mm and the operating speed of 10 km h⁻¹, the operating angle increases from 0° to 45°, and the power increases from 0.154 kW to 0.244 kW, with a growth rate of 58.44%. Therefore, the operating speed has a significant impact on the power. When the operating speed is constant, the power increases with the increase of operating depth and operating angle. At the operating speed of 7 km h⁻¹ and the operating depth of 60 mm, the operating angle increases from 0° to 45°, and the power increases from 0.079 kW to 0.139 kW, with a growth rate of 75.95%. At the operating speed of 7 km h⁻¹ and the operating depth of 80 mm, the operating angle increases from 0° to 45°, and the power increases from 0.124 kW to 0.192 kW, with a growth rate of 54.84%. Therefore, the operating depth has a significant impact on the power parameters. When the operating angle is constant, the power increases with the increase of operating depth and operating speed. At the operating angle of 22.5° and the operating depth of 60 mm, the power increases from 0.052 kW to 0.148 kW when the operating speed increases from 6 km h⁻¹ to 10 km h⁻¹, with a growth rate of 184.62%. At the operating angle of 22.5° and operating depth of 80 mm, the power increases from 0.081 kW to 0.217 kW when the operating speed increases from 6 km h⁻¹ to 10 km h⁻¹, with a growth rate of 167.90%. Therefore, the operating depth has significant impact on power parameters. At the operating angle of 22.5° and operating speed of 6 km h⁻¹, the power increases from 0.052 kW to 0.081 kW as the operating depth increases from 60 mm to 80 mm, with a growth rate of 55.77%. At the operating angle of 22.5° and operating speed of 8 km h⁻¹, the power increases from 0.092 kW to 0.141 kW as the operating depth increases from 60 mm to 80 mm, with a growth rate of 53.26%. Therefore, operating speed has more significant impact than operating depth, and the greater the operating speed, the smaller the influence of power consumption with the increase of operating depth.

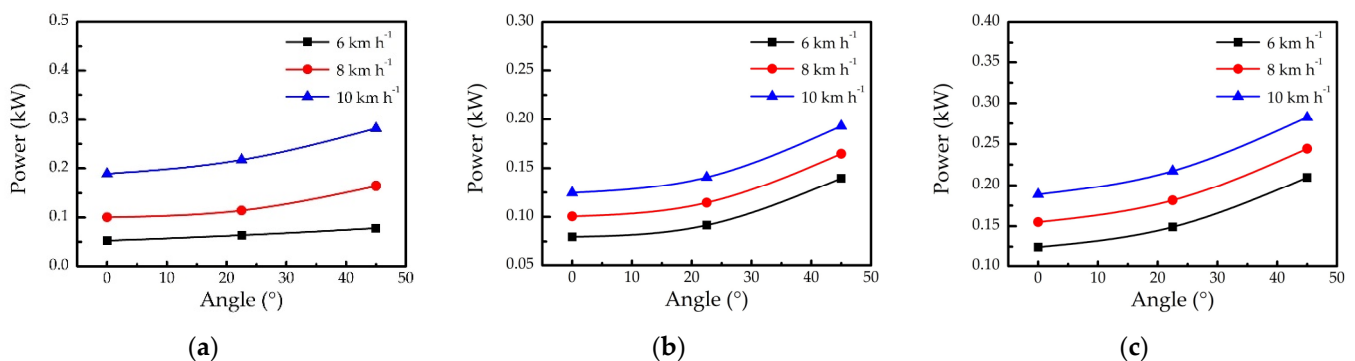


Figure 8. The relationship between power, operating angle, operating depth and operating speed. (a) The relationship between operating angle, operating speed and power at the operating depth of 60 mm. (b) The relationship between operating angle, operating speed and power at the operating depth of 70 mm. (c) The relationship between operating angle, operating speed and power at the operating depth of 80 mm.

3.4. The Relationship between Specific Energy Consumption, Operating Angle, Operating Depth and Operating Speed

As shown in Figure 9a–c, when the operating depth remains constant, the specific energy consumption decreases first and then increases with the increase of operating speed and increases with the increase of operating angle. At the operating depth of 70 mm and the operating speed of 6 km h⁻¹, the specific energy consumption decreases from 5.216 kJ m⁻³ to 4.289 kJ m⁻³, with a reduction rate of 17.79%, when the operating angle increases from 0° to 45°. At the operating depth of 70 mm and the operating speed of 10 km h⁻¹, when the operating angle increases from 0° to 45°, the specific energy consumption increases

from 5.050 kJ m^{-3} to 9.592 kJ m^{-3} , with a growth rate of 89.94%. Therefore, the operating speed has a significant impact on the power parameters. When the operating speed remains constant, the specific energy consumption increases with the increase of operating depth. At the operating speed of 7 km h^{-1} and the operating depth of 60 mm, when the operating angle increases from 0° to 45° , the specific energy consumption increases from 3.818 kJ m^{-3} to 5.926 kJ m^{-3} , with a growth rate of 55.21%. At the operating speed of 7 km h^{-1} and the operating depth of 80 mm, when the operating angle increases from 0° to 45° , the specific energy consumption increases from 3.631 kJ m^{-3} to 5.138 kJ m^{-3} , with a growth rate of 41.503%. Therefore, the operating depth has a significant impact on the specific energy consumption parameters. When the operating angle remains constant, the specific energy consumption increases with the increase of operating speed and increases first and then decreases with the increase of operating depth. At the operating angle of 22.5° and operating speed of 6 km h^{-1} , the specific energy consumption decreases from 395.09 kJ m^{-3} to $348.195 \text{ kJ m}^{-3}$ when the operating depth increases from 60 mm to 80 mm, with a reduction rate of 11.87%. Therefore, operating speed has a more significant impact than operating depth, and the smaller the operating depth, the greater the impact of specific energy consumption from the increase of operating speed.

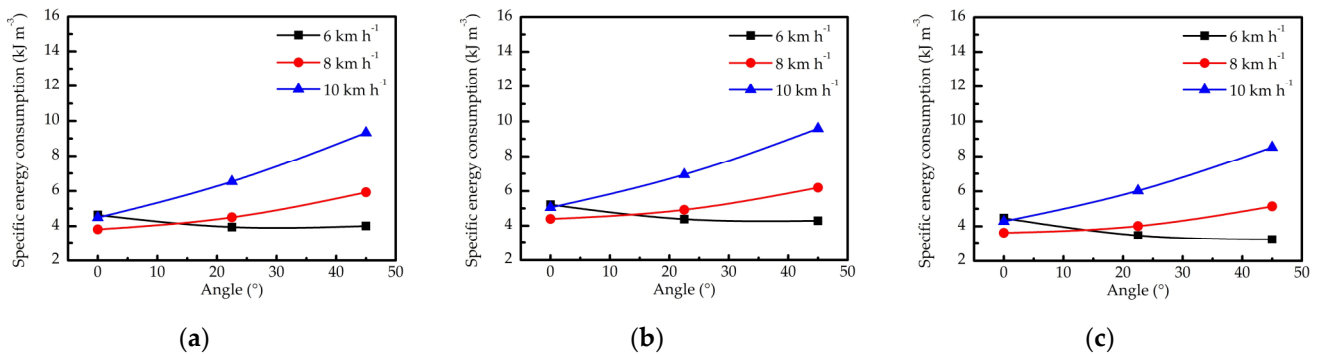


Figure 9. Relationship between specific energy consumption and penetration angle, operating depth and operating speed: (a) Relationship between penetration angle, operating speed and specific energy consumption at the operating depth of 60 mm; (b) relationship between penetration angle, operating speed and specific energy consumption at the operating depth of 70 mm; (c) relationship between penetration angle, operating speed and specific energy consumption at the operating depth of 80 mm.

Table 2 shows that both regression models can solve the optimal solutions of the parameters. Using Design-Expert software, the lowest power and the lowest specific energy consumption were taken as the solution conditions. The optimal combination of parameters obtained from Equations (3) and (4) is: operating depth of 60 mm, operating speed of 6 km h^{-1} , operating angle of 24.8° ; the power consumption under this operating condition is 0.053 kW, and the specific energy consumption is 392.55 kJ m^{-3} . The virtual simulation verification was conducted according to the optimization results; the power consumption is 0.058 kW, and the specific energy consumption is 4.017 kJ m^{-3} , which is basically consistent with the optimization results.

According to the selected range and the F -value of each factor on the results, it can be concluded that, for the parameters of power and specific energy consumption, the weight order of influencing factors is as follows: operating speed, operating angle and operating depth.

$$P = 0.2565 - 3.0818 \times 10^{-3}A - 0.0465B - 3.9914 \times 10^{-3}C + 2.8075 \times 10^{-4}AB + 9.2882 \times 10^{-6}AC + 4.8764 \times 10^{-4}BC + 3.5809 \times 10^{-5}A^2 + 2.1980 \times 10^{-3}B^2 + 1.6670 \times 10^{-5}C^2 \quad (3)$$

$$Q = -15.6241 - 0.1892A - 2.9815B + 0.9267C + 0.0304AB - 0.0007AC - 0.0005BC + 0.00071A^2 + 0.1858B^2 - 0.0067C^2 \quad (4)$$

Table 2. Optimization model of test data.

Resources	Regression Model on Power				Regression Model on Specific Energy Consumption			
	Sum of Squares	df	F-Value	p-Value	Sum of Squares	df	F-Value	p-Value
Model	0.043	9	4.769×10^{-3}	<0.0001	32.36	9	505.26	<0.0001
A	8.233×10^{-3}	1	8.233×10^{-3}	<0.0001	6.53	1	918.26	<0.0001
B	0.027	1	0.027	<0.0001	13.20	1	1854.39	<0.0001
C	4.802×10^{-3}	1	4.802×10^{-3}	<0.0001	0.48	1	66.81	<0.0001
AB	6.384×10^{-4}	1	6.384×10^{-4}	0.0001	7.48	1	1051.49	<0.0001
AC	1.747×10^{-5}	1	1.747×10^{-5}	0.2474	0.09	1	12.69	0.0092
BC	3.800×10^{-4}	1	3.800×10^{-4}	0.0006	3.47×10^{-4}	1	0.049	0.8316
A ²	1.384×10^{-3}	1	1.384×10^{-3}	<0.0001	0.58	1	81.39	<0.0001
B ²	3.255×10^{-4}	1	3.255×10^{-4}	0.0010	2.33	1	326.72	<0.0001
C ²	1.170×10^{-5}	1	1.170×10^{-5}	0.3361	1.87	1	262.41	<0.0001
Residual	7.680×10^{-5}	7	1.097×10^{-5}		0.05	7		
Lack of Fit	6.774×10^{-5}	3	2.258×10^{-5}	0.0251	0.041	3	6.45	0.0517
Pure Error	9.062×10^{-6}	4	2.265×10^{-6}	<0.0001	8.53×10^{-3}	4		
Cor Total	0.043	16			32.41	16		

3.5. Soil Bin Verification Test Results

In order to verify the accuracy of the parameter setting of the DEM virtual simulation model and the rationality of the parameter optimization of the bionic liquid fertilizer deep application spray needle, an indoor soil bin verification test was carried out at the depth of 60 mm and the operating speed of 6 km h^{-1} . The test was repeated for three groups, and the average value was taken as the test results. Extract the operating resistance and furrow profile of the bionic liquid fertilizer deep application spray needle after operation, respectively, and the test results are shown in Table 3.

Table 3. Comparison of DEM virtual simulation test results with indoor soil bin test results.

Test Form	No.	Power (kW)	Specific Energy Consumption (kJ m^{-3})
DEM virtual simulation test	1	0.058	4.017
	2	0.067	4.438
Soil bin test results	3	0.058	4.335
	4	0.072	3.987
	Average value	0.066	4.257

The relative error between the DEM virtual simulation test and the soil bin verification test is 13.80%. The relative error of specific energy consumption is 5.88%. The results of the DEM virtual simulation test and the soil bin verification test are basically consistent.

4. Discussion

4.1. Analysis of Soil Disturbance Behavior of Bionic Liquid Fertilizer Deep Application Spray Needle

The bionic liquid fertilizer spray needle cuts the soil in the process of operation, while crushing, squeezing and destroying the soil. Therefore, the resistance generated during the operation of the bionic liquid fertilizer deep application spray needle comes from the resistance generated by the bionic surface cutting the soil, the flow of soil along the bionic surface and the resistance generated [34,35].

4.1.1. Resistance of the Bionic Surface to the Soil Cutting Process

As shown in Figure 10a–c, the operation of the bionic liquid fertilizer deep application spray needle causes the soil to break down in a passive mode, creating a unit soil wedge of width dl and depth h [36]. Then, the liquid fertilizer deep application spray needle cutting soil generates traction force $-dF_c$, unit soil wedge gravity $-dF_G$, and unit soil wedge shear strength $-dR$.

$$dF_c \cos\left(\frac{\pi}{4} - \frac{\Psi}{2}\right) - dF_G \cos\left(\frac{\pi}{4} - \frac{\Psi}{2}\right) = dR \quad (5)$$

where Ψ is the angle of internal friction of the soil, rad. F_c is the unit soil wedge pressure generated during soil cutting, N. dF_G is the gravity of the unit soil wedge, N. dR is the shear resistance of the unit soil wedge, N.

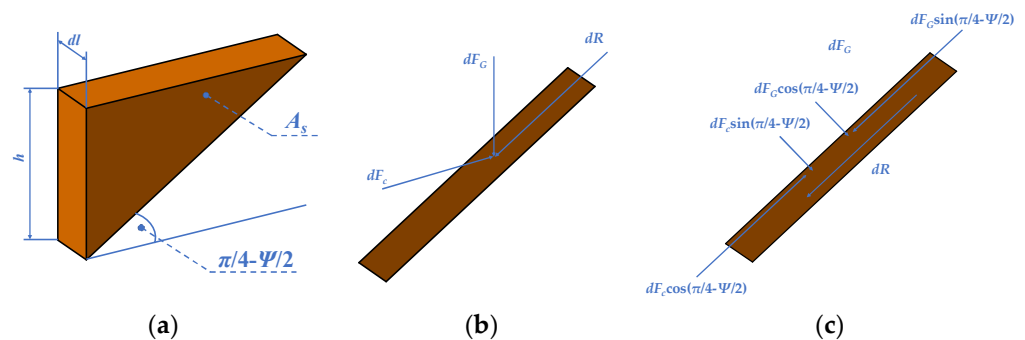


Figure 10. Force of unit soil wedge. (a) Unit soil wedge; (b) section of unit soil wedge; (c) force decomposition in the vertical and parallel slip plane.

The gravity of unit soil wedge is calculated by Equation (6):

$$dF_G = \rho_s g dV_s = \rho_s g dl A_s = \frac{\rho_s g dl h^2}{2 \tan\left(\frac{\pi}{4} - \frac{\Psi}{2}\right)} \quad (6)$$

where ρ_s is the density of the soil wedge; $g \text{ cm}^{-3}$. dV is the volume of the unit soil wedge, cm^{-3} ; and A_s is the cross-sectional area of the unit soil wedge, cm^{-2} .

The shear resistance of the unit soil wedge is calculated by Equation (7).

$$\begin{aligned} dR &= cdA_s + dF \tan \Psi \\ &= \frac{chdl}{\sin\left(\frac{\pi}{4} - \frac{\Psi}{2}\right)} + \left[dF_c \sin\left(\frac{\pi}{4} - \frac{\Psi}{2}\right) + dF_G \cos\left(\frac{\pi}{4} - \frac{\Psi}{2}\right) \right] \tan \Psi \end{aligned} \quad (7)$$

where c is the Soil cohesion force, Pa.

According to Equation (7), it can be seen that the shear resistance of the unit soil wedge is related to the soil wedge characteristics, which are related to the type and depth of the soil. Therefore, the resistance of the bionic surface to soil cutting is affected by soil type and the operating depth.

4.1.2. Resistance of Soil Flowing along the Bionic Surface

During the operation of the bionic liquid fertilizer deep application spray needle, the flowing state of the cutting soil on the bionic surface is the continuous motion, and the soil force on the bionic surface is calculated. The operation of the bionic liquid fertilizer deep application spray needle is regarded as uniform linear motion. Observed from the side view, when the soil unit contacts the surface curve of the bionic liquid fertilizer deep application spray needle, there are operating resistance F_v and relative velocity v , respectively, which are decomposed along the coordinate axis into tangential velocity v_τ and normal velocity v_n , wherein the normal velocity v_n is all converted into operating resistance F . The resistance F can be decomposed into horizontal operating resistance F_x and vertical operating resistance F_y , and the pressure generated by the vertical resistance on the bionic surface is the friction

force. Dynamic analysis of the interaction between the bionic surface and the soil unit is conducted, as shown in Figure 11 and Equation (8).

$$F = ma = \frac{m(v_\tau - v_0)}{t} \quad (8)$$

where m is the mass of the soil unit, kg. a is the acceleration of the soil unit, $m\ s^{-2}$. v_0 is the forward end velocity, $m\ s^{-1}$, t is the operating time, s.

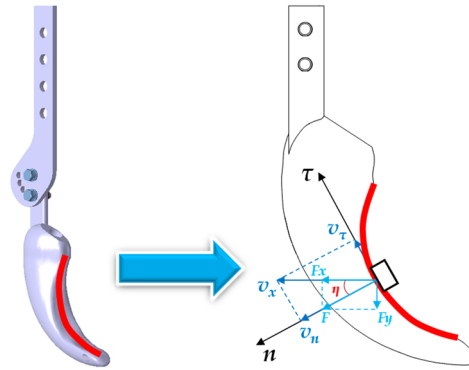


Figure 11. Kinetic analysis of the interaction between the bionic liquid fertilizer deep application spray needle surface and soil unit.

F_v on the surface of the bionic liquid fertilizer deep application spray needle is composed of horizontal resistance F_x and vertical resistance F_y . The vertical resistance F_y produces positive pressure on the bionic surface, which is also represented by the friction force F_f . The forward resistance F_v on the bionic liquid fertilizer deep application spray needle is composed of the horizontal operating resistance F_x and the horizontal component F_{fx} of friction F_f .

$$F_v = F \cos \eta = \frac{m(v_\tau - v_0) \cos \eta}{t} = \frac{mv \cos^2 \eta}{t} \quad (9)$$

$$F_{fx} = \mu F_y \sin^2 \eta = \mu F \sin^3 \eta \quad (10)$$

$$v_n = v_x \cos \eta \quad (11)$$

$$F_v = F_x + F_{fx} = \frac{mv \cos \eta}{t} (\mu \sin^3 \eta + \cos \eta) \quad (12)$$

where η is the angle between the operating speed v_x and the normal direction, $^\circ$. μ , is the friction factor between the surface of the bionic liquid fertilizer deep application spray needle and the soil.

Equation (12) shows that the resistance generated by soil flow along the bionic surface is affected by the operating speed and angle [37].

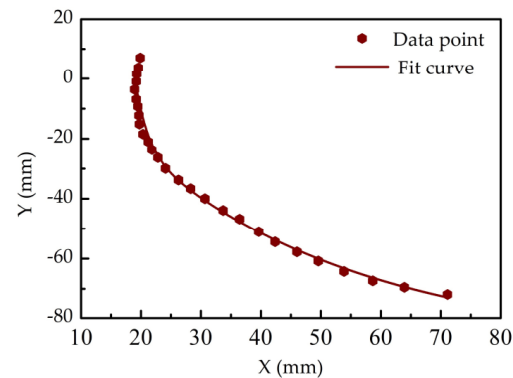
In summary, the operating resistance of the bionic liquid fertilizer deep application spray needle mainly comes from the cutting of soil by bionic surface structure, the flow of soil along the bionic surface and the resistance generated, which is related to the type of soil, operating depth, speed and angle.

4.2. Analysis of Soil Disturbance Behavior of Deep Application of Bionic Liquid Fertilizer Spray Needles

In order to determine the structural parameters of the inner side of the liquid fertilizer deep application spray needle and to facilitate analysis, the points were first taken with the inner claw-toe curve of the fertilizer spray needle, and the coordinate data were obtained. The obtained data were imported into Origin Pro software for curve fitting, and the fitting equation of the bionic surface structure curve of the liquid fertilizer deep application spray needle was obtained, as shown in Table 4. The curve fitting image is shown in Figure 12.

Table 4. Curve fitting results.

Fitting Equation	R^2
$y = 110.28e^{-\frac{x}{37.45}} + 184853.84e^{-\frac{x}{2.11}}$	0.95815

**Figure 12.** Fitting curve of the bionic surface of the bionic liquid fertilizer deep application spray needle.

The specific energy consumption test index of the bionic liquid fertilizer deep application spray needle operation mainly depends on the operating resistance and soil disturbance area. The bionic structure has the characteristics of multi-extreme value points on the surface curve, which can significantly reduce the operating power and specific energy consumption. The liquid fertilizer deep application furrow opener in literature [24] was selected for comparison under the same operating conditions (operating depth of 80 mm, operating speed of 6 km h⁻¹). The parameters of power consumption and specific energy consumption were calculated, and the results were shown in Table 5.

Table 5. Comparison between DEM virtual simulation test results and indoor soil bin test results.

No.	Soil-Engaging Component	Power (kW)	Specific Energy Consumption (kJ m ⁻³)
1	Biological liquid fertilizer deep application spray needle ($A = 24.8^\circ$)	0.084	3.421
2	Core-share opener (Su_0)	0.118	7.010
3	Biological sturgeon liquid fertilizer deep application opener (Su_1)	0.106	10.186
4	Biological sturgeon liquid fertilizer deep application opener (Su_2)	0.112	10.557
5	Biological sturgeon liquid fertilizer deep application opener (Su_3)	0.095	8.558
6	Biological sturgeon liquid fertilizer deep application opener (Su_4)	0.092	6.634

It can be seen from the results that the bionic liquid fertilizer deep application spray needle has superior operating performance.

According to Equation (13), $\mu \sin^3 \eta$ is much smaller than $\cos \eta$, so the equation can be simplified as Equation (14):

$$F_v' = \frac{mv \cos^2 \eta}{t} \quad (13)$$

Since η is the angle between the operating speed v_x and the normal direction angle, the angle between the tangential line of the contact point of the bionic fertilizer deep application spray needle surface structure and the soil unit is $(90^\circ - \eta)$, of which the tangent value is the

differential value of the curve equation in Table 4 at this point. The total resistance of the curve is the integral of $\sum F_v'$ within the range of x , and the resultant force is:

$$\Sigma F_v' = \int_0^x F_v' dx_i = \int_0^x \frac{mv}{t} \left(\left(\frac{d_{xi}}{d_{yi}} \right)^2 + 1 \right)^{-1} d \left(\frac{d_{xi}}{d_{yi}} \right) \quad (14)$$

According to Equation (14), the horizontal operating resistance was calculated when the surface curves of the furrow opener were straight line, circular arcs and bionic curves: bionic curve < circular arc < straight line, and the results show that the bionic curve of the badger claw-toe structure has excellent performance in reducing the operating resistance [38].

5. Conclusions

In this research, we found that the bionic liquid fertilizer deep application needle has the characteristics of low power consumption and low specific energy consumption, and the key parameters affecting its operating performance are operating speed, penetration angle and operating depth. The best parameter combination applicable to northeast China is: The operating depth is 60 mm; the operating speed is 6 km h⁻¹; and the operating angle is 24.8°. The DEM virtual simulation test results under this operating condition are the power of 0.058 kW and the specific energy consumption of 4.017 kJ m⁻³. The test results of indoor soil bin test are the power of 0.066 kW and the specific energy consumption of 4.257 kJ m⁻³. The relative error of DEM virtual simulation test is 13% and 5.88%, which has high accuracy.

In this research, we established a mechanical and kinematic model of the interaction process between the surface curve of the bionic liquid fertilizer deep application spray needle and the soil, which can provide a theoretical basis for the future design of the bionic fertilizer spray needle.

In this research, compared with other liquid fertilizer deep application furrow openers, the bionic design of liquid fertilizer deep application spray needle has superior operating performance with 9.52~40.5% reduction in power parameters and 93.9~208.6% reduction in specific energy consumption parameters.

In this research, the bionic design of the liquid fertilizer deep application spray needle can effectively replicate the low resistance and low friction characteristics of the burrowing animal claw-toe structure to the liquid fertilizer deep application spray needle. Therefore, this design method can provide an effective means for the future field of liquid fertilizer deep application touchdown component design.

In this research, we only conducted tests and studies for soil conditions in the cold regions of northeast China, and further in-depth studies on soil suitability in other regions will be conducted in the future, which is conducive to promoting the use of liquid fertilizer and protecting the valuable black land resources.

Author Contributions: Conceptualization, W.Z. and Y.W.; methodology, X.N.; software, N.W.; formal analysis, T.A.; resources, Y.W.; writing—original draft preparation, W.Z.; writing—review and editing, Y.W.; funding acquisition, Y.W. All authors have read and agreed to the published version of the manuscript.

Funding: This research was financially supported by the National key research and development program (No.2022YFD2001401-02), Heilongjiang Provincial Natural Science Foundation of China (No. JJ2022YX0432), Hei Long Jiang Postdoctoral Foundation (No.LBH-TZ2211).

Institutional Review Board Statement: Not applicable.

Data Availability Statement: Not applicable.

Acknowledgments: The authors would like to thank their schools and colleges, as well as the funding providers of the project, and thanks to Li Xiang for supporting this research. All support and assistance are sincerely appreciated.

Conflicts of Interest: The authors declare no conflict of interest.

Nomenclature

A	Operating angle of bionic liquid fertilizer deep application spray needle
B	Operating speed of bionic liquid fertilizer deep application spray needle
C	Operating depth of bionic liquid fertilizer deep application spray needle
P	Operating power of bionic liquid fertilizer deep application spray needle
Q	Operating specific energy consumption of bionic liquid fertilizer deep application spray needle
v	Operating speed of bionic liquid fertilizer deep application spray needle
F	Average operating horizontal resistance of bionic liquid fertilizer deep application spray needle in the data collection area
W	Operating energy consumption of bionic liquid fertilizer deep application spray needle in the data collection area.
V	Volume of soil disturbance of the operation of bionic liquid fertilizer deep application spray needle
L	Operating distance of bionic liquid fertilizer deep application spray needle
S	Soil disturbance cross-sectional area of bionic liquid fertilizer deep application spray needle
dl	Width of unit soil wedge
h	Depth of unit soil wedge
dF_G	(N) Gravity of unit soil wedge
dR	Shear resistance of unit soil wedge
ρ_s	Density of soil wedge
dV	Volume of unit soil wedge
A_s	Cross-sectional area of unit soil wedge
F_c	Unit soil wedge pressure during soil cutting with bionic liquid fertilizer deep application spray needle
F_v	Unit soil wedge resistance of bionic liquid fertilizer deep application spray needle
F_v'	Unit soil wedge resistance after the simplification of bionic liquid fertilizer deep application spray needle
$\sum F_v'$	Resistance of bionic liquid fertilizer deep application
v_τ	Tangential velocity of soil unit
v_n	Normal velocity of soil unit
F_x	Resistance in x direction of unit soil wedge on surface of bionic liquid fertilizer deep application spray needle
F_y	Resistance in y direction of unit soil wedge on surface of bionic liquid fertilizer deep application spray needle
F_f	Friction force F_f of soil wedge on surface of bionic liquid fertilizer deep application spray needle
F_{fx}	Horizontal component of F_f
η	Angle between unit soil wedging operating velocity v_x and normal direction
μ	Friction coefficient between surface of bionic liquid fertilizer deep application spray needle and soil
Ψ	Internal friction angle of soil
m	Soil unit mass
a	Acceleration of soil unit
v_0	Forward end velocity of soil unit
t	operating time

References

1. Teng, Y.; Pang, B.; Guo, X. Study on the quality improvement on black land in Northeast China under the environment of sustainable agricultural development. *Kybernetes* **2021**. [CrossRef]
2. Xu, X.Z.; Xu, Y.; Chen, S.C.; Xu, S.G.; Zhang, H.W. Soil loss and conservation in the black soil region of Northeast China: A retrospective study. *Environ. Sci. Policy* **2010**, *13*, 793–800. [CrossRef]

3. Liu, Y.; He, M.; Wang, Y.; Sun, Y.; Gao, X. Farmland Aerial Images Fast-Stitching Method and Application Based on Improved SIFT Algorithm. *IEEE Access* **2022**, *10*, 95411–95424. [[CrossRef](#)]
4. Han, T.; Jinwu, W.; Changsu, X.U.; Wenqi, Z.; Jinfeng, W.; Xiu, W. Research progress analysis on key technology of chemical fertilizer reduction and efficiency increase. *Nongye Jixie Xuebao/Trans. Chin. Soc. Agric. Mach.* **2019**, *50*, 1–19.
5. Li, T.; Zhang, Y.; Bei, S.; Li, X.; Reinsch, S.; Zhang, H.; Zhang, J. Contrasting impacts of manure and inorganic fertilizer applications for nine years on soil organic carbon and its labile fractions in bulk soil and soil aggregates. *Catena* **2020**, *194*, 104739. [[CrossRef](#)]
6. Sithole, N.J.; Magwaza, L.S.; Thibaud, G.R. Long-term impact of no-till conservation agriculture and N-fertilizer on soil aggregate stability, infiltration and distribution of C in different size fractions. *Soil Tillage Res.* **2019**, *190*, 147–156. [[CrossRef](#)]
7. Fan, J.; Ding, W.; Ziadi, N. Thirty-year manuring and fertilization effects on heavy metals in black soil and soil aggregates in northeastern China. *Commun. Soil Sci. Plant Anal.* **2013**, *44*, 1224–1241. [[CrossRef](#)]
8. Guo, Y.; Luo, L.; Chen, G.; Kou, Y.; Xu, H. Mitigating nitrous oxide emissions from a maize-cropping black soil in northeast China by a combination of reducing chemical N fertilizer application and applying manure in autumn. *Soil Sci. Plant Nutr.* **2013**, *59*, 392–402. [[CrossRef](#)]
9. Zhang, J.; An, T.; Chi, F.; Wei, D.; Zhou, B.; Hao, X.; Jin, L.; Wang, J. Evolution over years of structural characteristics of humic acids in Black Soil as a function of various fertilization treatments. *J. Soils Sediments* **2019**, *19*, 1959–1969. [[CrossRef](#)]
10. Zhou, W.; Wen, N.; Liu, Z.; Wang, Q.; Tang, H.; Wang, J.; Wang, J. Research on an Efficient Deep-Hole Application Method for Liquid Fertilizer Based on Alternate Drilling. *Processes* **2022**, *10*, 1320. [[CrossRef](#)]
11. Martinova, N.; Shavazov, K.; Telovov, N.; Toigambayev, S.; Yusupov, S. Machine for carrying works on deep loosening of soil with the simultaneous application of liquid organic fertilizers. In *IOP Conference Series: Earth and Environmental Science*; IOP Publishing: Bristol, UK, 2020; p. 012145.
12. Zhou, W.; Song, C.; Sun, X.; Liu, Z.; Ni, X.; Shen, K.; Wang, Y.J.; Tian, L. Design of High-Efficiency Soil-Returning Liquid Fertilizer Deep-Application Furrow Openers for Improving Furrowing Performance in Cold Regions of Northeast China. *Agriculture* **2022**, *12*, 1286. [[CrossRef](#)]
13. Tong, J.; Moayad, B.Z.; Ma, Y.-h.; Sun, J.-y.; Chen, D.-h.; Jia, H.-l.; Ren, L.-q. Effects of biomimetic surface designs on furrow opener performance. *J. Bionic Eng.* **2009**, *6*, 280–289. [[CrossRef](#)]
14. Jarecki, M.K.; Parkin, T.B.; Chan, A.S.K.; Kaspar, T.C.; Moorman, T.B.; Singer, J.W.; Kerr, B.J.; Hatfield, J.L.; Jones, R. Cover crop effects on nitrous oxide emission from a manure-treated Mollisol. *Agric. Ecosyst. Environ.* **2009**, *134*, 29–35. [[CrossRef](#)]
15. Hang, C.; Huang, Y.; Zhu, R. Analysis of the movement behaviour of soil between subsoilers based on the discrete element method. *J. Terramechanics* **2017**, *74*, 35–43. [[CrossRef](#)]
16. Ren, L.; Liang, Y. Biological couplings: Classification and characteristic rules. *Sci. China Ser. E Technol. Sci.* **2009**, *52*, 2791–2800. [[CrossRef](#)]
17. Jia, H.; Zheng, J.; Zhao, J.; Guo, M.; Zhuang, J.; Wang, Z. Design and parameter optimization of earthworm-like multi-function opener. *Trans. Chin. Soc. Agric. Eng.* **2018**, *34*, 62–71.
18. Huang, S.; Hu, Y.; Wang, Y. Research on aerodynamic performance of a novel dolphin head-shaped bionic airfoil. *Energy* **2021**, *214*, 118179. [[CrossRef](#)]
19. Ma, Y.; Pei, G.; Wang, H.; Lü, X.; Song, G.; Tong, J. Simulation and experiment of badger claw toe bionic excavator bucket tooth for improving performance of digging and cutting. *Trans. Chin. Soc. Agric. Eng.* **2016**, *32*, 67–72.
20. Guan, C.; Fu, J.; Xu, L.; Jiang, X.; Wang, S.; Cui, Z. Study on the reduction of soil adhesion and tillage force of bionic cutter teeth in secondary soil crushing. *Biosyst. Eng.* **2022**, *213*, 133–147. [[CrossRef](#)]
21. Shuhong, Z.; Hongjun, L.; Hewen, T. Design and performance experiment of opener based on bionic sailfish head curve. *Trans. Chin. Soc. Agric. Eng. (Trans. Csa)* **2017**, *33*, 32–39.
22. Wang, Y.; Xue, W.; Ma, Y.; Tong, J.; Liu, X.; Sun, J. DEM and soil bin study on a biomimetic disc furrow opener. *Comput. Electron. Agric.* **2019**, *156*, 209–216. [[CrossRef](#)]
23. Lee, J.; Tirtawardhana, C.; Myung, H. Development and analysis of digging and soil removing mechanisms for mole-bot: Bio-inspired mole-like drilling robot. In Proceedings of the 2020 IEEE/RSJ International Conference on Intelligent Robots and Systems (IROS), Las Vegas, NV, USA, 25–29 October 2020; IEEE: Piscataway, NJ, USA, 2020; pp. 7792–7799.
24. Wang, J.; Wen, N.; Liu, Z.; Zhou, W.; Tang, H.; Wang, Q.; Wang, J. Coupled Bionic Design of Liquid Fertilizer Deep Application Type Opener Based on Sturgeon Streamline to Enhance Opening Performance in Cold Soils of Northeast China. *Agriculture* **2022**, *12*, 615. [[CrossRef](#)]
25. Sun, J.; Chen, H.; Wang, Z.; Ou, Z.; Yang, Z.; Duan, J. Study on plowing performance of EDEM low-resistance animal bionic device based on red soil. *Soil Tillage Res.* **2020**, *196*, 104336. [[CrossRef](#)]
26. Barr, J.; Desbiolles, J.; Ucgul, M.; Fielke, J.M. Bentleg furrow opener performance analysis using the discrete element method. *Biosyst. Eng.* **2020**, *189*, 99–115. [[CrossRef](#)]
27. Barr, J.B.; Ucgul, M.; Desbiolles, J.M.A.; Fielke, J.M. Simulating the effect of rake angle on narrow opener performance with the discrete element method. *Biosyst. Eng.* **2018**, *171*, 1–15. [[CrossRef](#)]
28. Hongfa, X.; Houji, L.; Xiaoming, W. A preliminary study of the sets of badger in Yancheng nature reserve. *Shou Lei Xue Bao= Acta Theriol. Sin.* **1997**, *17*, 107–112.
29. Gu, Z.X.; Zheng, W.C. Hole digging kinematic image acquisition of badger's forelimb digging hole. *J. Econ. Anim.* **2013**, *17*, 152–154.

30. Ji, W.; Chen, D.; Jia, H.; Tong, J. Experimental investigation into soil-cutting performance of the claws of mole rat (*Scaptochirus moschatus*). *J. Bionic Eng.* **2010**, *7*, S166–S171. [[CrossRef](#)]
31. Jinwu, W.; Ziming, L.I.U.; Xiaobo, S.U.N.; Han, T.; Qi, W.; Wenqi, Z. Design and Experiment of Fertilizing Device for Deep Application of Liquid Fertilizer with Target Fertilizing System. *Trans. Chin. Soc. Agric. Mach.* **2022**, *53*, 152–162.
32. Wang, J.; Ji, W.; Feng, J.; Wang, J. Design and experimental investigation of the liquid fertilizer applicator. *Trans. Csa* **2008**, *24*, 157–159.
33. Aikins, K.A.; Ucgul, M.; Barr, J.B.; Jensen, T.A.; Antille, D.L.; Desbiolles, J.M.A. Determination of discrete element model parameters for a cohesive soil and validation through narrow point opener performance analysis. *Soil Tillage Res.* **2021**, *213*, 105123. [[CrossRef](#)]
34. Ahmadi, I. Development and assessment of a draft force calculator for disk plow using the laws of classical mechanics. *Soil Tillage Res.* **2016**, *163*, 32–40. [[CrossRef](#)]
35. Obermayr, M.; Dressler, K.; Vrettos, C.; Eberhard, P. Prediction of draft forces in cohesionless soil with the Discrete Element Method. *J. Terramechanics* **2011**, *48*, 347–358. [[CrossRef](#)]
36. Fanhao, M. *Bionic Design and Experiment of Sliding Opening Device*; Jilin University: Changchun City, China, 2021.
37. Jinwu, W.; Xiang, L.I.; Pengxiang, G.A.O.; Mingjun, N.A.; QiZ, W.; Wenqi, H.O.U. Design and Experiment of High Efficiency Drag Reducing Shovel for Carrot Combine Harvester. *Nongye Jixie Xuebao/Trans. Chin. Soc. Agric. Mach.* **2020**, *51*, 93–103.
38. Liu, S.; Weng, S.; Liao, Y.; Zhu, D. Structural bionic design for digging shovel of cassava harvester considering soil mechanics. *Appl. Bionics Biomech.* **2014**, *11*, 1–11. [[CrossRef](#)]

Disclaimer/Publisher’s Note: The statements, opinions and data contained in all publications are solely those of the individual author(s) and contributor(s) and not of MDPI and/or the editor(s). MDPI and/or the editor(s) disclaim responsibility for any injury to people or property resulting from any ideas, methods, instructions or products referred to in the content.